IEEE Photonics Journal
An IEEE Photonics Society Publication

Open Access

Theoretical Modeling of 4.3 μm Mid-Infrared Lasing in Dy^{3+}-Doped Chalcogenide Fiber Lasers

Volume 10, Number 2, April 2018

Xusheng Xiao
Yantao Xu
Haitao Guo
Pengfei Wang
Xiaoxia Cui
Min Lu
Yishan Wang
Bo Peng

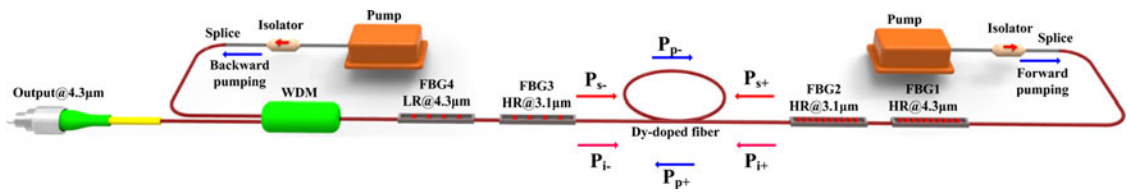

DOI: 10.1109/JPHOT.2018.2803155
1943-0655 © 2018 IEEE

Theoretical Modeling of 4.3 μm Mid-Infrared Lasing in Dy^{3+}-Doped Chalcogenide Fiber Lasers

Xusheng Xiao,[1] **Yantao Xu**,[1,2] **Haitao Guo**,[1] **Pengfei Wang**,[1] **Xiaoxia Cui**,[1] **Min Lu**,[1] **Yishan Wang**,[1] **and Bo Peng**[1]

[1]State Key Laboratory of Transient Optics and Photonics, Xi'an Institute of Optics and Precision Mechanics, Chinese Academy of Sciences, Xi'an 710119, China
[2]Graduate School of Chinese Academy of Sciences, Beijing 100049, China

DOI:10.1109/JPHOT.2018.2803155
1943-0655 © 2018 IEEE. Translations and content mining are permitted for academic research only. Personal use is also permitted, but republication/redistribution requires IEEE permission. See http://www.ieee.org/publications_standards/publications/rights/index.html for more information.

Manuscript received July 20, 2017; revised January 23, 2018; accepted February 3, 2018. Date of publication February 7, 2018; date of current version February 23, 2018. This work was supported in part by the National Nature Science Foundation of China under Grants 61475189 and 61405241 and in part by the West Light Foundation from Chinese Academy of Science of China. Corresponding author: Haitao Guo (e-mail: guoht_001@opt.ac.cn).

Abstract: We theoretically investigate a Dy^{3+}-doped chalcogenide fiber lasers operating at 4.3 μm based on the rate equations and propagation equations. The two main pump bands for 1319 and 1707 nm corresponding to the ${}^6H_{15/2} \rightarrow {}^6H_{9/2}$ and ${}^6H_{15/2} \rightarrow {}^6H_{13/2}$ transitions are discussed in detail. The predicted maximum slope efficiencies are determined to be $\sim$7.8% and $\sim$15.1% for the two pumping wavelength, respectively. Besides, the variety of laser performance has been systematically analyzed when the pump configurations, fiber length, fiber loss are varied. This numerical analysis might be useful to explore the 4.3 μm lasing operation for the mid-infrared chalcogenide fiber lasers in future.

Index Terms: Theoretical modeling, fiber lasers, 4.3 μm mid-infrared.

1. Introduction

Rare-earth (RE) ions doped fiber laser sources operating at mid-infrared (MIR) regions are of great interests due to their potential applications in many areas such as chemical sensing, medical surgery, national defense, and etc [1]–[3]. As an example, many greenhouse and atmosphere gases exhibit fundamental vibrational absorption in the 4.3 μm band region, which promote its application including global warming monitoring, carbon cycle studies and combustion diagnostics [4]–[8]. Currently, quantum cascade lasers (QCLs) [4], [5] and optical parametric oscillator (OPO) [6] are popularly used as light sources at this MIR wavelength. However, they show inevitable disadvantages in some cases including of beam quality, power scaling, narrow linewidth, and etc. In contrast, fiber lasers can make up for these deficiencies.

Among several RE ions, the Dy^{3+} presents an emission band centered at 4.3 μm corresponding to the transition between the ${}^6H_{11/2}$ and ${}^6H_{13/2}$ levels, which can be exploited for the laser operation near 4.3 μm wavelength. However, the energy transition of ${}^6H_{11/2} \rightarrow {}^6H_{13/2}$ is self-terminated due to that the lifetime of lower laser level (${}^6H_{13/2}$) is $\sim$3 times as large as that of upper one (${}^6H_{11/2}$) [10]–[13]. The cascade lasing corresponding to the ${}^6H_{11/2} \rightarrow {}^6H_{13/2}$ and ${}^6H_{13/2} \rightarrow {}^6H_{15/2}$ transitions

can effectively eliminate this self-terminated behavior and achieve an efficient laser output without saturation [22], [23]. Laser generation at 4.3 μm has been successfully achieved from Dy^{3+} ions doped chalcogenide crystals such as $PbGa_2S_4$ [12]–[16].

For achieving compact, reliable and continuous-wave (CW) operated MIR lasers with low cost and high power, fiber lasers based on Dy^{3+} ions doped glass fiber are raised. A few theoretical works have been reported before [22]–[25], and the active material is focused on the Dy^{3+} ions doped chalcogendie glass fiber (DDCF). Compared to silica glass ($\sim$1100 cm^{-1}) and fluoride one ($\sim$560 cm^{-1}), the lower phonon energy of chalcogenide glass ($\sim$300–450 cm^{-1}) leads to a decrease in multi-phonon relaxation rates [9], [10], which allows radiative transitions between RE ion's levels in the $\geq$4 μm MIR range. In 2008, Quimby *et al.* [22] have demonstrated a numerical modeling of the cascade lasing in DDCF laser with efficient output at 4.5 μm. Similarly, a simple DDCF laser designed for MIR light generation was investigated in 2010 [23], however, its cascaded Fabry-Perot cavities was provided by Fresnel light reflection at glass fiber-air interfaces without the need of fiber grating fabrication. What's more, in 2016, Mario *et al.* [25] illustrated an efficient single lasing output at 4.3 μm based on a photonic crystal fiber made of Dy^{3+} ions doped chalcogenide glass.

Though 4.3 μm fiber laser based on the DDCF has not been realized until now, many bottleneck problems have been paid attention and resolved step by step. Some chalcogenide glass fibers with high Dy^{3+} ions concentration were designed and fabricated [32], [33]. The chalcogenide glass fiber-based optical component have been also developed rapidly [17]–[21]. In [17], two nested pairs of fiber Bragg gratings were efficiently inscribed in a low-loss As_2S_3 fiber and its reflected wavelength centered at 3.34 and 3.77 μm respectively. Based on this formed cascaded Fabry-Perot cavities, the 3.77 μm output wavelength was generated. In addition, the Naval Research Laboratory has demonstrated N $\times$ 1 chalcogenide-fiber based combiners in 2013 [19]. Meanwhile, the low-loss, robust fusion splicing of these dissimilar fibers were achieved by the Naval Research Laboratory [20]. All these make it possible to develop 4.3 μm mid-infrared all-fiber cascade laser based on DDCF.

As we all know, the Dy^{3+} transition ${}^6H_{11/2} \rightarrow {}^6H_{13/2}$ corresponding to the generated radiation at $\sim$4.3 μm can be excited either at 1.32 μm (pumping to the ${}^6H_{9/2}$ energy level) or at the wavelength of $\sim$1.7 μm (directly to the ${}^6H_{11/2}$ level). Unfortunately, the effect of the pumping wavelength and configuration on the laser performance have not been studied before. Besides, some important laser parameters, such as signal gain and pump absorption coefficient, have been rarely discussed. In this investigation, we theoretically present our numerical simulation studies on a 4.3 μm all-fiber laser based on Dy^{3+} ions doped $Ge_5Ga_{20}Sb_{10}S_{65}$ chalcogenide glass fiber. The effects of pump wavelengths and active fiber features as well as pump configurations on the laser performance have been systematically investigated to optimize the operation of fiber lasers. Our calculations show that the preferable laser performance was achieved when the fiber laser was pumped by 1707 nm compared to pumping of 1319 nm. Furthermore, the reason on the saturation of signal laser without idler was quantitatively analyzed in detail.

2. Numerical Model

Separate numerical models are constructed containing the rate equations and propagation equations for each pump scheme. Homogeneous broadening is used, namely, the number of ions in one level is the same for different wavelengths [29]. The pump wavelengths are close to the peak value of the two main absorption bands. Note that the criterion for selecting the suitable pumping wavelength is to find the best compromise between the absorption cross-section and the available output power of corresponding laser sources. Therefore, a commercial 1319 nm semiconductor laser and a home-made Tm^{3+} doped silicate fiber laser operating at 1707 nm [34] are choose as pump sources in this work. Fig. 1 shows a schematic illustration of the cascade DDCF laser. In the laser structure, the output fiber end-face is considered to be handled with bevel treatment to eliminate any residual broadband feedback and suppress parasitic lasing.

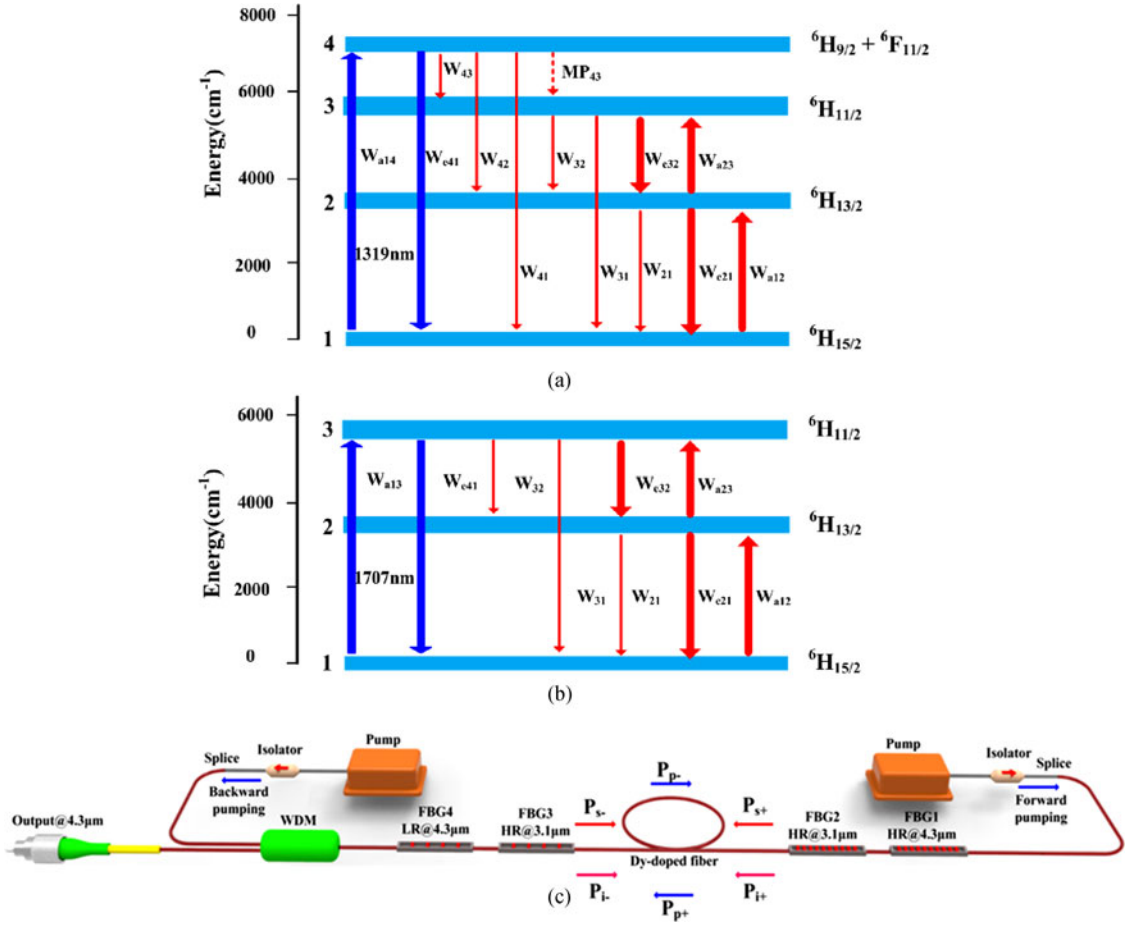

Fig. 1. (a) Simplified energy diagram of the four lower levels of Dy^{3+}: 1319 nm pumping scheme. (b) Simplified energy diagram of the three lower levels of Dy^{3+}: 1707 nm pumping scheme. (c) Cascade lasing scheme with simultaneous lasing at $\lambda_s = \sim 4300$ nm and $\lambda_i = \sim 3100$ nm. FBG: fiber bragg grating; WDM: wavelength division multiplexor.

2.1 $^6H_{15/2} \rightarrow {}^6H_{9/2} + {}^6F_{11/2}$ Pump Scheme: 1319 nm Pumping

The energy diagram of the four lower levels of Dy^{3+} is shown in Fig. 1(a). The diagram shows the spontaneous transitions (thin lines), stimulated emission and absorption transitions (thick lines) between each pair of levels. It is worth mentioning that the $^6H_{13/2} \rightarrow {}^6H_{5/2}$ pump excited-state absorption (ESA) process (this transition has resonance with $^6H_{15/2} \rightarrow {}^6H_{9/2}$ ground-state absorption transition) is negligible in the calculation because its cross-section is far less than ground-state absorption cross-section. The rate equations and propagation equations for the four-level system can be written as:

$$\frac{dN_4}{dt} = N_1 W_{a14} - N_4 (W_{e41} + W_{43} + W_{42} + W_{41} + M P_{43})$$
$$\frac{dN_3}{dt} = N_2 W_{a23} - N_3 (W_{32} + W_{31} + W_{e32}) + N_4 (W_{43} + M P_{43})$$
$$\frac{dN_2}{dt} = N_1 W_{a12} - N_2 (W_{21} + W_{e21} + W_{a23}) + N_3 (W_{32} + W_{e32}) + N_4 W_{42}$$
$$N = N_1 + N_2 + N_3 + N_4 \quad (1a)$$

$$\pm\frac{dP_{p\pm}(v,z)}{dz} = \left(\mp\Gamma_p(v)*(\sigma_{14}(\lambda)*N_1(z)-\sigma_{41}(\lambda)*N_4(z))\mp\alpha_p\right)P_{p\pm}(v,z)$$
$$\pm\frac{dP_{s\pm}(v,z)}{dz} = (\mp\Gamma_s(v)*(\sigma_{23}(\lambda)*N_2(z)-\sigma_{32}(\lambda)*N_3(z))\mp\alpha_s)P_{s\pm}(v,z)$$
$$\pm\frac{dP_{i\pm}(v,z)}{dz} = (\mp\Gamma_i(v)*(\sigma_{12}(\lambda)*N_1(z)-\sigma_{21}(\lambda)*N_2(z))\mp\alpha_i)P_{i\pm}(v,z) \quad (2a)$$

2.2 $^6H_{15/2} \rightarrow {}^6H_{11/2}$ Pump Scheme: 1707 nm Pumping

The energy diagram of the three lower levels of Dy^{3+} is shown in Fig. 1(b). We assume direct pumping into the upper laser level $^6H_{11/2}$ with a Tm^{3+} ions doped fiber laser at 1.707 μm. The rate equations and propagation equations for the three-level system can be written as:

$$\frac{dN_3}{dt} = N_1W_{a13}+N_2W_{a23}-N_3(W_{e41}+W_{32}+W_{31}+W_{e32})$$
$$\frac{dN_2}{dt} = N_1W_{a12}-N_2(W_{21}+W_{e21}+W_{a23})+N_3(W_{32}+W_{e32})$$
$$N = N_1+N_2+N_3 \quad (1b)$$

$$\pm\frac{dP_{p\pm}(v,z)}{dz} = \left(\mp\Gamma_p(v)*(\sigma_{13}(\lambda)*N_1(z)-\sigma_{31}(\lambda)*N_3(z))\mp\alpha_p\right)P_{p\pm}(v,z)$$
$$\pm\frac{dP_{s\pm}(v,z)}{dz} = (\mp\Gamma_s(v)*(\sigma_{23}(\lambda)*N_2(z)-\sigma_{32}(\lambda)*N_3(z))\mp\alpha_s)P_{s\pm}(v,z)$$
$$\pm\frac{dP_{i\pm}(v,z)}{dz} = (\mp\Gamma_i(v)*(\sigma_{12}(\lambda)*N_1(z)-\sigma_{21}(\lambda)*N_2(z))\mp\alpha_i)P_{i\pm}(v,z) \quad (2b)$$

In the above-mentioned equations ((1.a) and (1.b)), N_k is the number of ions in level k, k = 1–4, N is the density of Dy^{3+} ions, and the subscript a and e denote absorption and emission, respectively. The MP_{43} is the multi-phonon decay rate between level 4 and 3. The spontaneous transition probability per unit time between i and level j is denoted as W_{ij}. β_{ij} is the branching ratio for the $i \rightarrow j$ transition. The lifetime of level j is τ_j and the total spontaneous decay rate of level j is denoted as $W_j = 1/\tau_j$. The stimulated rate between level i and j are given by

$$W_{xij} = \sum P(v)\sigma_{ij}(\lambda)\Gamma(v)/Ahv \quad (3)$$

Where Σ indicates the sum over all the frequencies, x = a or e, $P(v)$ is the power, $\sigma_{ij}(\lambda)$ is the cross-section between level i and j, $\Gamma(v)$ is the fractional overlap of the mode intensity with the ion-doped core, and A is the fiber's core area.

In the above equations ((2.a) and (2.b)), $P_p \pm (v,z)$, $P_s \pm (v,z)$ and $P_i \pm (v,z)$ are the pump light, signal light and idler light powers which propagate along the positive (subscript "+") or negative (subscript "−") z direction ($0 \le z \le L$, L is the length of active fiber), respectively. α_p, α_s and α_i represent the propagation loss of the pump light, signal light and idler light in the active fiber, respectively, where we assumed that α is independent of the location z and wavelength for simplicity. The powers at pump light, signal light and idler light are propagated back and forth between the FBGs, which are subject to the following boundary conditions at the fiber ends:

$$P_{p+} = P_p^f P_{p-} = P_p^b$$
$$P_{s+}(0) = R_1P_{s-}(0)\ P_{s-}(L) = R_2P_{s+}(L)$$
$$P_{i+}(0) = R_3P_{i-}(0)\ P_{i-}(L) = R_4P_{i+}(L) \quad (4)$$

TABLE 1
Dy^{3+} Ions Doped $Ge_{20}Ga_5Sb_{10}S_{65}$ Chalcogenide Fiber Laser Model Parameters

Symbol	Value	Unit	Symbol	Value	Unit
λ_{p1}	1319	nm	τ_4	0.04	ms
λ_{p2}	1707	nm	τ_3	6.2	ms
λ_s	4300	nm	τ_2	2	ms
λ_i	3100	nm	β_{43}	0.01	_
σ_{41}	$16.4 * 10^{-21}$	cm^2	β_{42}	0.12	_
σ_{14}	$16.4 * 10^{-21}$	cm^2	β_{32}	0.15	_
σ_{31}	$6.0 * 10^{-21}$	cm^2	MP_{43}	19000	s^{-1}
σ_{13}	$6.3 * 10^{-21}$	cm^2	Γ_p	0.034	_
σ_{32}	$9.2 * 10^{-21}$	cm^2	Γ_s	0.82	_
σ_{23}	$6.0 * 10^{-21}$	cm^2	Γ_i	0.9	_
σ_{21}	$3.5 * 10^{-21}$	cm^2	N	$6.0 * 1019$	cm^{-3}
σ_{12}	$1.0 * 10^{-21}$	cm^2	α	1/4.343	cm^{-1}
A_c	$0.95 * 10^{-6}$	cm^2	R1	0.99	_
R_{core}	5.5	μm	R2	0.99	_
R_{clad1}	30	μm	R3	0.9	_
R_{clad2}	62.5	μm	R4	0.2	_

where P_p^f and P_p^b are the pump powers coupled into the fiber from the forward and backward directions, respectively. $R_{j(j=1-4)}$ are the power peak reflectivities of the correspondent FBGs at respective wavelength. For CW laser operation, we obtain the steady-state solution to ((1.a) and (1.b)) by setting $dN_k/dt = 0$, and $k = 1 - 4$. Equations (1)–(2) are coupled, which should be solved iteratively with a convergence criterion that tests the convergence of the overall signal power. We solve the above equations by fourth-order Runge-Kutta algorithm [27], [28], [30] and the related optical parameters obtained from [9], [11], [25] are listed in Table 1. In this modeling, taking into account the feasibility of laser design, we assume the dysprosium concentration is 6×10^{19} ions/cm^3. The $Ge_{20}Ga_5Sb_{10}S_{65}$ fiber doped with 6×10^{19} ions/cm^3 of Dy^{3+} allows to achieve a favorable compromise for easy implementation of fiber drawing, optical attenuation and fluorescence [31]. To avoid the deleterious nonlinear effect, the maximum pump power is set to 3 W.

3. Results and Discussions

The effects of active fiber length on output power for different pump powers in a forward pumping configuration are shown in Fig. 2. In the case of 1319 nm pumping (see Fig. 2(a)), the calculated output power at 4.3 μm displays a significant enhancing with increasing fiber length when $L \leq 1.2$ m, which indicates that the gain was presented in dominant position compared to the overall intrinsic loss. With further increase of the fiber length, the laser output power starts to decrease due to the combined effect of pump depletion and the cumulative fiber loss. Thus, the optimal active fiber length is between 1.0 and 1.5 m. Similarly, in the case of 1707 nm pumping (see Fig. 2(b)), the calculated output power is observed to display similar trends as observed for 1319 nm pumping, and the optimal interval of fiber length increases to 1.6–2.2 m. The variation in the predicted slope efficiency and threshold pump power for the two pumping wavelength when the active fiber length is varied is displayed in Fig. 3. In the case of 1319 nm pumping (see Fig. 3(a)), the predicted slope

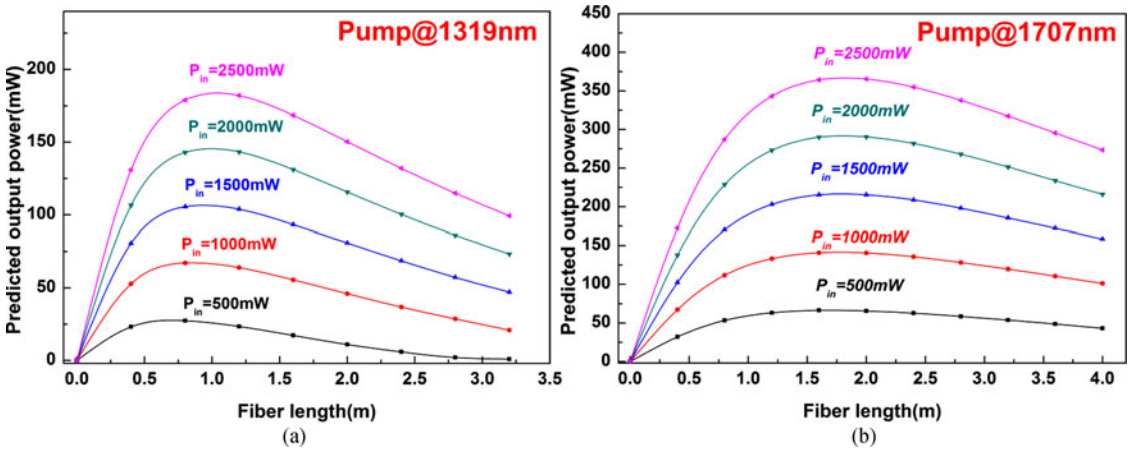

Fig. 2. The output power versus the fiber length for different pump power in (a) the 1319 nm pumping scheme and (b) the 1707 nm pumping scheme.

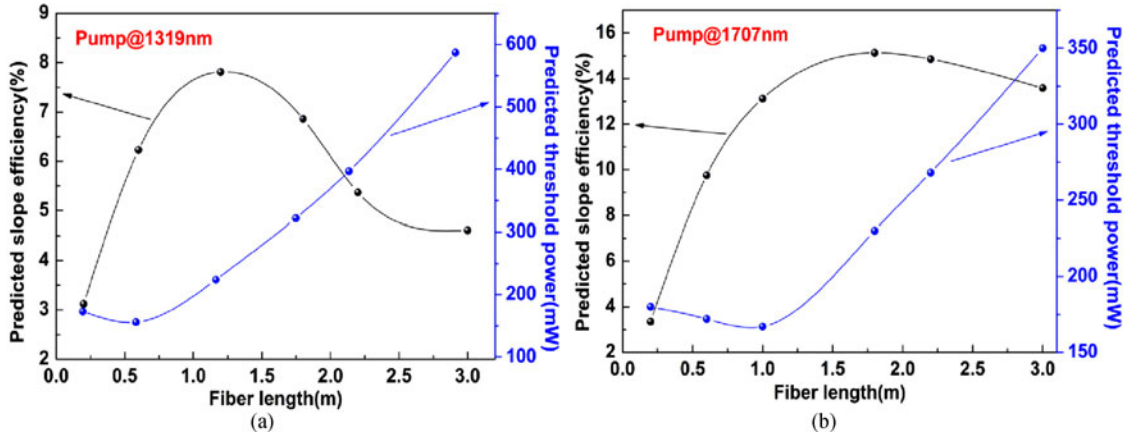

Fig. 3. The predicted slope efficiency and threshold power versus the fiber length in (a) the 1319 nm pumping scheme and (b) the 1707 nm pumping scheme.

efficiency displays a maximum value of ~7.8% for fiber length ranges between 1.0 m and 1.2 m, and the predicted threshold displays a minimum value of ~156 mW when the fiber length is 0.6 m. Overall, the varying curve for the slope efficiency shows an expected tendency to increase first and then decrease with the increase of fiber length and the threshold curve shows the opposite trend. In the case of 1707 nm pumping (see Fig. 3(b)), the similar varying curves for the calculated slope efficiency and threshold pump power are obtained. However, the maximum slope efficiency is significantly improved by 2 times to ~15.1% for fiber length of ~1.8 m.

Fig. 4 displays the predicted output power at 4.3 μm as a function of absorbed pump power for the two pumping wavelength with respective corresponding optimal fiber lengths when the idler lasing at 3100 nm exist or not. As can be seen from the figure, the predicted output power for the two pumping wavelength saturate at ~9.5 and ~60 mW respectively when the idler is off, ascribed to the self-termination limit of the ${}^6H_{11/2} \rightarrow {}^6H_{13/2}$ transition [12], [15]. To eliminate this negative effect, cascade laser [31] were carried out between the ${}^6H_{11/2} \rightarrow {}^6H_{13/2}$ and ${}^6H_{13/2} \rightarrow {}^6H_{15/2}$ transitions, i.e., the idler light at 3100 nm and the signal light at 4300 nm are co-lasing. As can be seen from Fig. 4, the expected linear increase of output power with the launched pump is found, which is attributed to the removal of self-termination limit. The predicted maximum slope efficiencies achieved by the two pumping wavelength are observed to be ~7.8% (1319 nm pumping) and ~15.1% (1707 nm pumping), respectively. Compared to the pumping of 1319 nm, the direct pumping into the up-

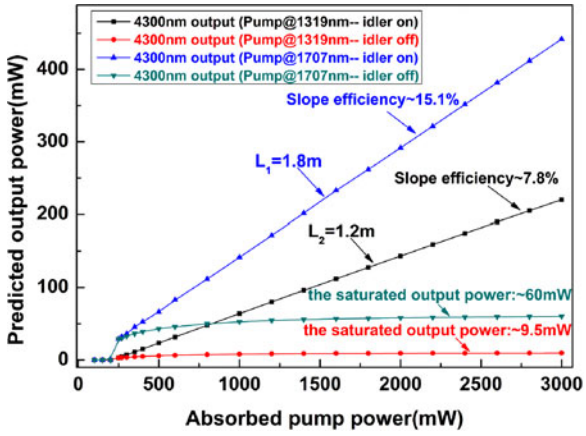

Fig. 4. The predicted output power at 4.3 μm as a function of absorbed pump power for the two pumping wavelengths.

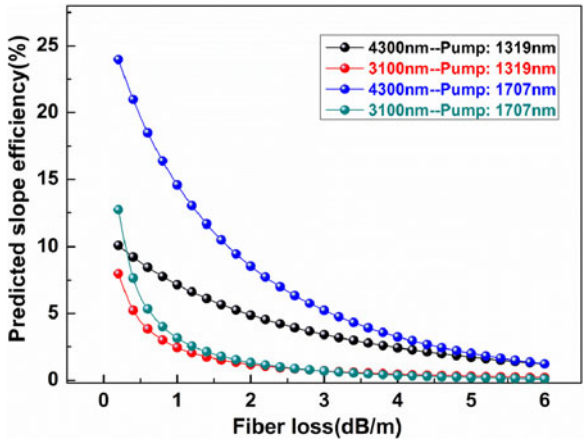

Fig. 5. The dependences of the predicted slope efficiency on the fiber loss for the signal and idler lights.

per laser level $^6H_{11/2}$ is achieved by pumping of 1707 nm, which greatly reduces quantum defect [14], [22]. Thus the better laser performance is observed and the corresponding slope efficiency is dramatically improved. Besides, benefited from the direct pumping, the saturation effect is relatively weaker.

Fig. 5 shows the dependences of the predicted slope efficiency on the fiber loss for the signal and idler light in the two pump schemes. As we can see, the output power at idler wavelength sharply drops to a negligible value of 0.1% when the fiber loss increases from 0.2 dB/m to 6 dB/m, which represents the cascade lasing operation will be blocked. Meanwhile, the predicted slope efficiencies decrease accordingly from 12.7% and 24.8% to 2.1% and 2.3% for the two pumping wavelengths, respectively. There is no doubt that further increase of the fiber loss will significantly quench the lasing. It is necessary to keep the fiber loss below 6 dB/m for achieving efficient lasing operation at 4.3 μm.

Fig. 6 shows the predicted output power at 4.3 μm versus absorbed pump power for various output reflectivities of FBG4. For the output reflectivities of 40%, 30%, 20% and 10%, the corresponding slope efficiencies are observed to be 12.4%, 13.6%, 15.1% and 16.2%, respectively. The thresholds are 176, 197, 234 and 267 mW, respectively. As can be seen from the calculations above, relatively high slope efficiency and threshold power can be obtained for a low output reflectivity. However, owing to the high Fresnel reflection of chalcogenide fiber end-face, it may lead to the generation of

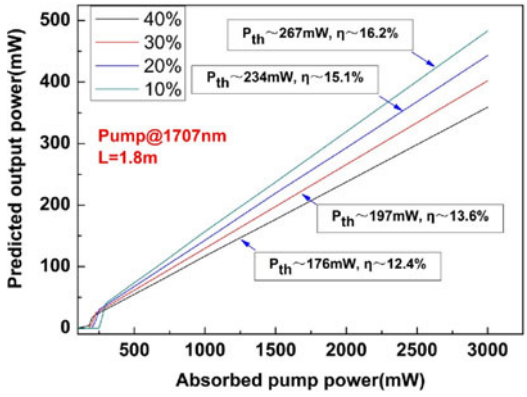

Fig. 6. The predicted output power versus the absorbed pump power for various output reflectivities of FBG4 for pumping of 1707 nm.

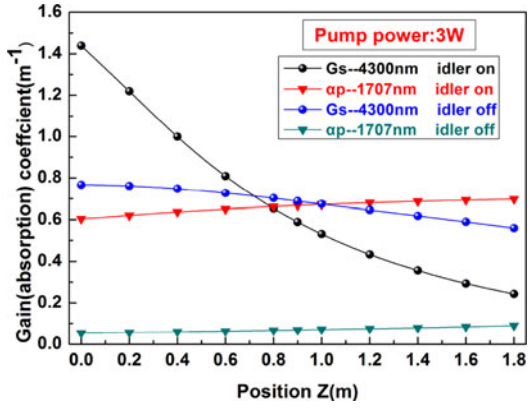

Fig. 7. The variations of the pump absorption and signal gain coefficients along the active fiber for the 1707 nm pumping.

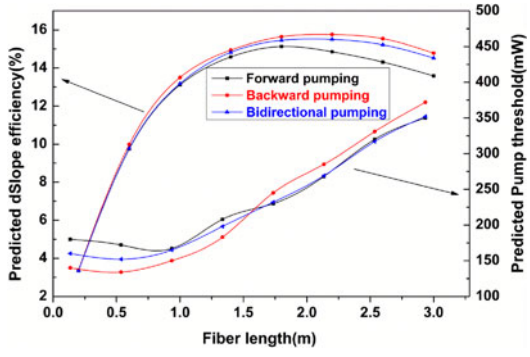

Fig. 8. The variation in the calculated slope efficiencies and threshold pump power for three different pump configurations when the fiber length is varied.

parasitic lasers for the relatively low output reflectivity. Thus, the output reflectivity of 20% is a good choice for achieving efficient lasing operation at 4.3 μm.

In order to explore the mechanism of laser self-termination, the variations of the pump absorption and signal gain coefficients along the active fiber under the forward pumping configuration for the 1707 nm one are displayed in Fig. 7. It can be seen that the pump absorption coefficient is dramatically reduced by 90% from ~0.6 to ~0.06 m^{-1} after the idler off, which is attributed to the stronger bleaching of the ground-state population. The pump bleaching mentioned above should be

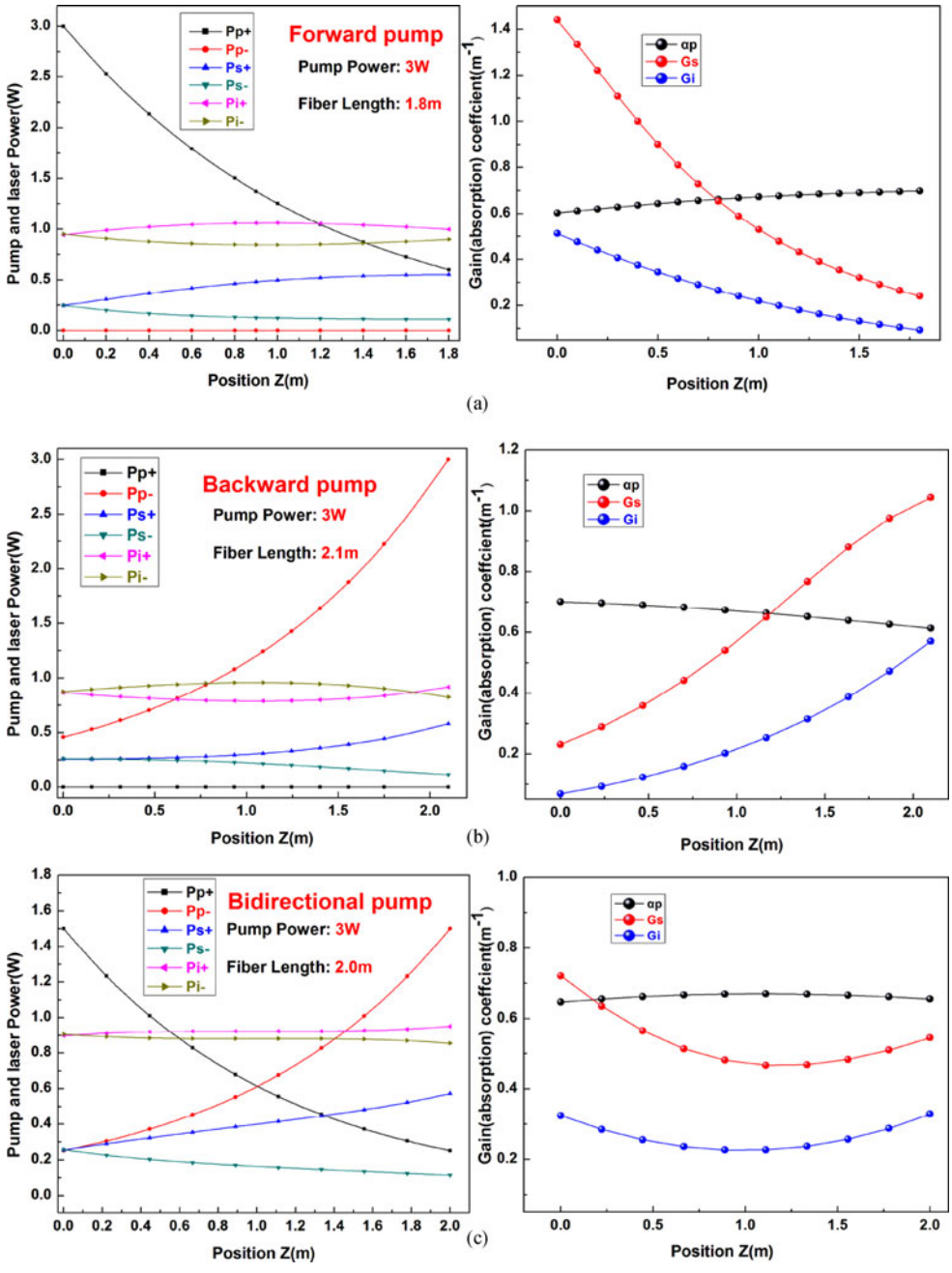

Fig. 9. The distributions of pump and laser powers (left), and gain (absorption) coefficient (right) along the active fiber under (a) forward pump configuration (b) backward pump configuration and (c) bidirectional pump configuration.

responsible for the laser self-terminated behavior, which lead to the saturation of the output power in the region of 60 mW. Thus, the cascade lasing on the loop ${}^6H_{11/2} \rightarrow {}^6H_{13/2} + {}^6H_{13/2} \rightarrow {}^6H_{15/2} => {}^6H_{15/2} \rightarrow {}^6H_{11/2}$ can activate the inhibited laser process and suppress the laser self-terminated behavior. Besides, the expected varying curves for the signal gain coefficient are observed and they decrease monotonically along the fiber length with the increase of signal light power. Benefited from the introduction of idler, the small signal gain coefficient is improved effectively from $\sim$0.78 to $\sim$1.45 m^{-1}.

In our simulation calculations, influence of pump configuration on laser performance in the 1707 nm pumping scheme is investigated in detail. The Fig. 8 displays the variations of the calculated slope efficiencies and threshold pump power for three different pump configurations when the fiber length is varied. Three varying curves for the calculated slope efficiencies are presented with the similar trends and the maximum slope efficiencies are ~15.1%, ~15.4% and ~15.8% for forward, bidirectional and backward pump configurations, respectively. Note that the optimum fiber lengths are slightly ascending for above three pump configurations. In aspect of the threshold pump power, the minimum value achieved are accordingly observed to be 175, 156 and 134 mW, respectively. What's more, the three corresponding curves show an interesting varying trend. When the fiber length is less than 1.8 m, the minimum threshold P_{th} under the three pumping configurations generally follow the trend of P_{th}(backward)$<$ P_{th}(bidirectional)$<$ P_{th}(forward). However, with the fiber length increasing further, an opposite varying trend is observed. Certainly, noting that the threshold of bidirectional pumping is basically the intermediate value achieved by other two pumping configurations, which is due to that the bidirectional pumping configuration is a combination of forward and backward pumping configurations.

Fig. 9 shows the distributions of pump and laser powers, and gain (absorption) coefficient along the active fiber under different pumping configurations. In this calculation, the launched pump power is set to 3 W and the fiber lengths are corresponding to their respective optimal values for the different pumping configurations. General speaking, the optimal fiber length is obtained in situations where the value of signal gain coefficient along the fiber is decreased to a comparative one of loss coefficient (Gs $= \alpha$s when un-directional pumping or Gs $= 2\alpha$s when bidirectional pumping), which can be verified from Fig. 8. The distribution curves about the power along the fiber show the same varying trend in the un-bidirectional pumping (forward or backward pumping). By contrast, using the bidirectional pumping can make the pump and laser power uniformly distributed throughout the active fiber, which is beneficial to achieve a lower thermal load and little nonlinear effect. Besides, the gain and absorption curves are more flat than those of un-bidirectional pumping ones. In terms of the slope efficiencies, a better performance is achieved by the backward pumping. However, we can't evaluate the pumping structure just from the point of laser performance. Instead, what should also be considered is the experimental feasibility and complexity of the laser design. As seen from Fig. 1(c), the backward and bidirectional pumping structures need the fabrication of the wavelength division multiplexor (WDM). In this respect, the forward pumping shows a distinct advantage to the others due to its more simple and feasible optical system.

4. Conclusion

In this work, we have systematically investigated the dependences of pump wavelengths and fiber features as well as pump configurations on the laser performance. The relative fiber laser performance when the fiber laser is pumped into each of the $^6H_{9/2}$ and $^6H_{11/2}$ absorption bands by 1319 and 1707 nm are comprehensively compared. The 1707 nm pumping was determined to be the most efficient, achieving a predicted slope efficiency of ~15.1% which is approximately twice that associated with 1319 nm pumping. It is also found that reasonable laser operation is expected for fiber loss below 6 dB/m. Furthermore, among the three pumping structures, each of them has its unique advantage and some unavoidable shortcomings, in which the backward and bidirectional pumping show relatively better laser performances, however, the forward pumping own a more simple and feasible optical system.

References

[1] S. D. Jackson, "Towards high-power mid-infrared emission from a fiber laser," *Nature Photon.*, vol. 6, pp. 423–431, 2012.

[2] F. Chenard and R. A. Kuis, "Chalcogenide fiber for mid-infrared transmission and generation of laser source," *Proc. SPIE*, vol. 7693, 2010, Art. no. 769308.

[3] N. Myoung, D. V. Martyshkin, V. V. Fedorov, and S. B. Mirov, "Energy scaling of 4.3 μm room temperature Fe:ZnSe laser," *Opt. Lett.*, vol. 36, pp. 94–96, 2011.

[4] Y. Yao, A. J. Hoffman and C. F. Gmachl, "Mid-infrared quantum cascade lasers," *Nature Photon.*, vol. 6, pp. 432–439, 2012.

[5] A. Harrer *et al.*, "4.3 μm quantum cascade detector in pixel configuration," *Opt. Express*, vol. 24, pp. 17041–17049, 2016.

[6] D. Chen and K. Masters, "Continuous-wave 4.3-μm intracavity difference frequency generation in an optical parametric oscillator," *Opt. Lett.*, vol. 26, pp. 25–27, 2001.

[7] R. V. Geldern *et al.*, "Field-based stable isotope analysis of carbon dioxide by mid-infrared laser spectroscopy for carbon capture and storage monitoring," *Anal. Chem.*, vol. 86, 2014, Art. no. 12198.

[8] W. Fub, W. E. Schmid, and K. L. Kompa, "3 W average power 4.3 μm CO_2 laser," *Opt. Quantum Electron.*, vol. 23, pp. 405–410, 1991.

[9] B. N. Samson, T. Schweizer, D. W. Hewak, and R. I. Laming, "Properties of dysprosium-doped gallium lanthanum sulfide fiber amplifiers operating at 1.3 μm," *Opt. Lett.*, vol. 22, pp. 703–705, 1997.

[10] L. B. Shaw, B. Cole, P. A. Thielen, J. S. Sanghera, and I. D. Aggarwal, "Mid-wave IR and long-wave IR laser potential of rare-earth doped chalcogenide glass fiber," *IEEE J. Quantum Elect.*, vol. 37, no. 9, pp. 1127–1137, Sep. 2001.

[11] V. G. Truong *et al.*, "Relaxation properties of rare-earth ions in sulfide glasses: Experiment and theory," *Phys. Rev. B*, vol. 74, 2006, Art. no. 184103.

[12] J. Šulc *et al.*, "Dysprosium-doped $PbGa_2S_4$ laser excited by diode-pumped Nd:YAG laser," *Opt. Lett.*, vol. 35, pp. 3051–3053, 2010.

[13] H. Jelinkova *et al.*, "Resonant pumping of dysprosium doped lead thiogallate by 1.71 m Er:YLF laser radiation," *Laser Phys. Lett.*, vol. 8, pp. 349–353, 2011.

[14] H. Jelinkova *et al.*, "Dysprosium-doped $PbGa_2S_4$ laser generating at 4.3 μm directly pumped by 1.7 μm laser diode," *Opt. Lett.*, vol. 38, pp. 3040–3043, 2013.

[15] H. Jelinkova *et al.*, "Dysprosium thiogallate laser: Source of mid-infrared radiation at 2.4, 4.3, and 5.4 μm," *Appl. Phys. A*, vol. 122, pp. 738–741, 2016.

[16] N. P. Barnes and R. E. Allen, "Room temperature Dy: YLF laser operation at 4.34 μm," *IEEE J. Quantum Elect.*, vol. 27, no. 2, pp. 277–282, Feb. 1991.

[17] M. Bernier, V. Fortin, M. El-Amraoui, Y. Messaddeq, and R. Vallée, "3.77 μm fiber laser based on cascaded Raman gain in a chalcogenide glass fiber," *Opt. Lett.*, vol. 39, pp. 2052–2055, 2014.

[18] L. E. Zou *et al.*, "Efficient inscription of Bragg gratings in As_2S_3 fibers using near bandgap light," *Opt. Lett.*, vol. 38, pp. 3850–3853, 2013.

[19] M. Bernier, V. Fortin, N. Caron, M. El-Amraoui, Y. Messaddeq, and R. Vallée, "Mid-infrared chalcogenide glass Raman fiber laser," *Opt. Lett.*, vol. 38, pp. 127–129, 2013.

[20] R. Thapa *et al.*, "Low-loss, robust fusion splicing of silica to chalcogenide fiber for integrated mid-infrared laser technology development," *Opt. Lett.*, vol. 40, pp. 5074–5077, 2015.

[21] R. R. Gattass, R. Thapa, F. H. Kung, L. E. Busse, L. B. Shaw, and J. S. Sanghera, "Review of infrared fiber-based components," *Appl. Opt.*, vol. 54, pp. F25–F34, 2015.

[22] R. S. Quimby, L. B. Shaw, J. S. Sanghera, and I. D. Aggarwal, "Modeling of cascade lasing in Dy: chalcogenide glass fiber laser with efficient output at 4.5 μm," *IEEE Photon. Technol. Lett.*, vol. 20, no. 2, pp. 123–125, Jan. 2008.

[23] S. Sujecki *et al.*, "Modelling of a simple Dy^{3+} doped chalcogenide glass fibre laser for mid-infrared light generation," *Opt. Quantum Electron.*, vol. 42, pp. 69–79, 2010.

[24] F. Prudenzano, L. Mescia, L. Allegretti, V. Moizan, V. Nazabal, and F. Smektala, "Theoretical study of cascade laser in erbium-doped chalcogenide glass fibers," *Opt. Mater.*, vol. 33, pp. 241–245, 2010.

[25] M. C. Falconi *et al.*, "Design of an efficient pumping scheme for mid-IR Dy^{3+}:$Ga_5Ge_{20}Sb_{10}S_{65}$ PCF fiber laser," *IEEE Photon. Technol. Lett.*, vol. 28, no. 18, pp. 1984–1987, Sep. 2016.

[26] M. C. Falconi *et al.*, "Dysprosium-doped chalcogenide master oscillator power amplifier (MOPA) for mid-IR emission," *J. Lightw. Technol.*, vol. 35, no. 2, pp. 265–273, Jan. 2017.

[27] S. D. Jackson and T. A. King, "Theoretical modeling of Tm-doped silica fiber lasers," *J. Lightw. Technol.*, vol. 17, no. 5, pp. 948–956, May 1999.

[28] I. Kelson and A. Hardy, "Optimization of strongly pumped fiber lasers," *J. Lightw. Technol.*, vol. 17, no. 5, pp. 891–897, May 1999.

[29] J. Hu, C. R. Menyuk, C. Wei, L. B. Shaw, J. S. Sanghera, and I. D. Aggarwal, "Highly efficient cascaded amplification using Pr^{3+}-doped mid-infrared chalcogenide fiber amplifiers," *Opt. Lett.*, vol. 40, pp. 3687–3690, 2015.

[30] W. H. Wang, L. X. Li, D. D. Chen, and Q. Y. Zhang, "Numerical analysis of 2.7 μm lasing in Er^{3+}-doped tellurite fiber lasers," *Sci. Rep.*, vol. 6, 2016, Art. no. 31761.

[31] M. Pollnau *et al.*, "150 mW unsaturated output power at 3 mm from a single-mode-fiber erbium cascade laser," *Appl. Phys. Lett.*, vol. 66, pp. 3564–3566, 1995.

[32] F. Starecki *et al.*, "Mid-IR optical sensor for CO_2 detection based on fluorescence absorbance of Dy^{3+}:$Ga_5Ge_{20}Sb_{10}S_{65}$ fibers," *Sens. Actuators B. Chem.*, vol. 207, pp. 518–525, 2015.

[33] Z. X. Wang *et al.*, "Synthesis and spectroscopy of high concentration dysprosium doped GeS_2-Ga_2S_3-CdI_2 chalcohalide glasses and fiber fabrication," *J. Alloy Compound*, vol. 692, pp. 1010–1017, 2017.

[34] X. S. Xiao *et al.*, "3 W narrow-linewidth ultra-short wavelength operation near 1707 nm in thulium-doped silica fiber laser with bidirectional pumping," *Appl. Phys. B.*, vol. 123, pp. 135–138, 2017.